

Stability and optoelectronic property of lead-free halide double perovskite $Cs_2B'BiI_6$ (B' = Li, Na and K)

Yunhui Liu(刘云辉), Wei Wang(王威), Feng Xiao(肖峰), Liangbin Xiong(熊良斌), and Xing Ming(明星)
Citation: Chin. Phys. B, 2021, 30 (**10**): 108102. DOI: 10.1088/1674-1056/ac05a5
Journal homepage: http://cpb.iphy.ac.cn; http://iopscience.iop.org/cpb

What follows is a list of articles you may be interested in

Two-step growth of VSe_2 films and their photoelectric properties

Yu Zeng(曾玉), Shengli Zhang(张生利), Xiuling Li(李秀玲), Jianping Ao(敖建平), Yun Sun(孙云), Wei Liu(刘玮), Fangfang Liu(刘芳芳), Peng Gao(高鹏), Yi Zhang(张毅)
Chin. Phys. B, 2019, 28 (**5**): 058101. DOI: 10.1088/1674-1056/28/5/058101

Carrier transport via V-shaped pits in InGaN/GaN MQW solar cells

Shitao Liu(刘诗涛), Zhijue Quan(全知觉), Li Wang(王立)
Chin. Phys. B, 2017, 26 (**3**): 038104. DOI: 10.1088/1674-1056/26/3/038104

Preparation of silver-coated glass frit and its application in silicon solar cells

Feng Xiang(向锋), Biyuan Li(李碧渊), Yingfen Li(黎应芬), Jian Zhou(周健), Weiping Gan(甘卫平)
Chin. Phys. B, 2016, 25 (**7**): 078110. DOI: 10.1088/1674-1056/25/7/078110

Improved performance of microcrystalline silicon solar cell with graded-band-gap silicon oxide buffer layer

Shi Zhen-Liang, Ji Yun, Yu Wei, Yang Yan-Bin, Cong Ri-Dong, Chen Ying-Juan, Li Xiao-Wei, Fu Guang-Sheng
Chin. Phys. B, 2015, 24 (**7**): 078105. DOI: 10.1088/1674-1056/24/7/078105

Influence of Ag and Sn incorporation in In_2S_3 thin films

Lin Ling-Yan, Yu Jin-Ling, Cheng Shu-Ying, Lu Pei-Min
Chin. Phys. B, 2015, 24 (**7**): 078103. DOI: 10.1088/1674-1056/24/7/078103

Stability and optoelectronic property of lead-free halide double perovskite $Cs_2B'BiI_6$ (B' = Li, Na and K)*

Yunhui Liu(刘云辉)[1], Wei Wang(王威)[1], Feng Xiao(肖峰)[1], Liangbin Xiong(熊良斌)[2,†], and Xing Ming(明星)[1,‡]

[1] College of Science, Guilin University of Technology, Guilin 541004, China

[2] School of Optoelectronic Engineering, Guangdong Polytechnic Normal University, Guangzhou 510665, China

(Received 30 March 2021; revised manuscript received 8 May 2021; accepted manuscript online 27 May 2021)

Although lead-based perovskite solar cells have achieved more than 25% power conversion efficiency, the toxicity of lead and instability are still urgent problems faced in industrial application. Lead-free halide double perovskite (DP) materials are promising candidates to resolve these issues. Based on the density functional theory, we explore the geometric stability, thermodynamic stability, mechanical stability, electronic structures, and optical properties of the $Cs_2B'BiI_6$ (B' = Li, Na and K) DP materials. By analyzing the tolerance factor and octahedral factor, we find the geometric stabilities of Cs_2NaBiI_6 and Cs_2KBiI_6 DPs are better than Cs_2LiBiI_6. By calculating the total energy, formation energy and decomposition energy, we propose that the most favorable structure of $Cs_2B'BiI_6$ is the orthorhombic phase, and Cs_2LiBiI_6 is less stable relative to the other two counterparts from an energetic viewpoint. Mechanical stability evaluations reveal that the orthorhombic Cs_2LiBiI_6 material is less stable relative to the isostructural Cs_2NaBiI_6 and Cs_2KBiI_6 DPs. The mechanical property calculations indicate that the $Cs_2B'BiI_6$ DPs possess good ductility, which can be used as flexible materials. Electronic structures and optical property calculations show that the orthorhombic $Cs_2B'BiI_6$ DPs have suitable band gap values, weaker exciton binding energies, and excellent optical absorption performance in the visible-light range. Based on the above comprehensive assessments, we can conclude that the orthorhombic Cs_2NaBiI_6 and Cs_2KBiI_6 DPs with good stability are promising candidates for solar cell applications.

Keywords: lead-free halide double perovskite, solar cells, stability, optoelectronic property

PACS: 81.05.Zx, 88.40.H−, 31.15.es, 71.15.Mb **DOI:** 10.1088/1674-1056/ac05a5

1. Introduction

Lead-based halide perovskites have revolutionized the development of solar cells in the past decade, achieving a conversion efficiency of more than 25%, which are superior to the polycrystalline silicon and thin-film photovoltaic solar cells.[1–3] Despite these impressive achievements, halide perovskites still face some unresolved disadvantages. The instability and toxicity of lead are obstacles to the industrial application of solar cells.[4–6] In order to solve these issues, it is significant to find stable and non-toxic perovskite alternates.[7,8] One simple strategy to obtain lead-free halide is replacing Pb^{2+} cations with other less toxic divalent metal ions Sn^{2+} or Ge^{2+} in the same IV group.[9] Unfortunately, the materials containing Sn^{2+} and Ge^{2+} ions are often destabilized by the oxidation of divalent ions to their corresponding 4+ states.[10] Another promising way is based on the replacement of two divalent Pb^{2+} ions with one monovalent B'^{+} and one trivalent B''^{3+} cation ($2Pb^{2+} \rightarrow B'^{+} + B''^{3+}$), generating $A_2^+B'^+B''^{3+}X_6$ (A and B' = Li, Na, K, Rb, Cs, Ag, Tl, etc.; B'' = Bi, Al, Ln, Ga, Fe, etc.; X = F, Cl, Br, I) compounds, named as double perovskite (DP), which maintain both the perovskite crystal structure and the charge neutrality.[11–18]

The $A_2^+B'^+B''^{3+}X_6$ DP materials can date back to the end of the 1960s, for example, $Cs_2NaBiCl_6$ and Cs_2KBiCl_6 have been synthesized for a long time, historically known as elpasolite with a face-center cubic structure and space group of $Fm\bar{3}m$.[19] The ferroelastic and ferroelectric phase transitions in elpasolites have attracted intensive attentions, while they have never been considered for photovoltaic applications at that time.[19–21] The Raman spectrum of $Cs_2NaBiCl_6$ indicates that the structures of the $BiCl_6$ and $NaCl_6$ are (nearly) octahedra.[22] The low-temperature lattice instability of $Cs_2NaBiCl_6$ is ascribed to the Cs^+ hole size.[23] In view of the tremendous interest in halide perovskites, the experimentally already synthesized all-inorganic halide DPs $Cs_2B'BiX_6$, such as $Cs_2AgBiCl_6$, $Cs_2AgBiBr_6$, $Cs_2NaBiCl_6$, and $Cs_2NaBiCl_6$ have received widespread attention recently.[17] Owning to good stability under ambient conditions, suitable band gap values, and excellent optical absorption at the visible-light range, the $Cs_2AgBiCl_6$ and $Cs_2AgBiBr_6$ have been put forward as promising alternatives to the lead halide perovskites in 2016.[24–26] Alternatively, $Cs_2NaBiCl_6$ possesses an indirect band gap of 3.41 eV and shows adjustably photoelectric properties by various ion doping.[27–30] A bright orange-red phosphor has been achieved

*Project supported by the National Natural Science Foundation of China (Grant No. 11864008) and Guangxi Natural Science Foundation, China (Grant Nos. 2018GXNSFAA138185, 2018AD19200, and 2019GXNSFGA245006).

†Corresponding author. E-mail: xiongliangbin@gpnu.edu.cn

‡Corresponding author. E-mail: mingxing@glut.edu.cn

© 2021 Chinese Physical Society and IOP Publishing Ltd

by doping Mn^{2+} ions into $Cs_2NaBiCl_6$ host, and a red shift of the optical absorption and excitation spectra has been observed through further chemical substitution of Cl^- ions with Br^- ions.[28] The indirect band gap can change to direct one by gradual substitution of Bi^{3+} with In^{3+} in $Cs_2NaBiCl_6$, and a strong orange-yellow photoluminescence was observed when doped with Mn^{2+}, and can be manipulated by the Bi^{3+}/In^{3+} ratios.[29] In addition, $Cs_2NaBiCl_6$ nanocrystals with different concentrations of doped ions have been synthesized, which show the excitonic absorption energy shifting from 3.82 eV to 3.48 eV by Ag^+ ions doping, leading to a significant improvement of photoluminescence quantum yield from 1.7% to 20%.[30]

Recently, another novel halide DP material of Cs_2NaBiI_6 has been synthesized for the first time by hydrothermal reaction.[31] Cs_2NaBiI_6 possesses a proper band gap of 1.66 eV, high stability in ambient air, and excellent optical absorption performances, which fulfil the requirements of photovoltaic applications. Cs_2NaBiI_6 has been successfully applied into a solar cell device, which simultaneously solves the key issues of toxicity and stability of the lead-based halide perovskites. Furthermore, compared with the wider band gap of $Cs_2NaBiCl_6$, the iodide Cs_2NaBiI_6 points out a promising direction to reduce the band gap of the halide DP materials.[32] High quality Cs_2NaBiI_6 films have been obtained by vacuum evaporation, which dramatically enhances the photovoltaic performance by post-treatment engineering.[33] Different from the cubic structure of the common DP materials [Fig. 1(a)], the x-ray diffraction pattern of Cs_2NaBiI_6 powder is consistent with that of the MA_2AgBiI_6, which crystallizes in an orthorhombic structure.[31,34] However, detailed crystal structure information has not been reported in these pioneer works.

First-principles calculations have been extensively employed to design a series of halide DPs,[7,8,11–18] assess the stability of the DPs,[35] and explore the electronic and optical properties of DPs.[36,37] Based on a hypothetical cubic DP structure, the calculated formation enthalpy of the cubic phase Cs_2NaBiI_6 is positive,[38] indicating it is thermodynamically unstable, which is obviously contradictory with the experimental fact. As shown in Fig. 1(a), most $A_2^+B'^+B''^{3+}X_6$ DPs adopt the rock salt sublattice as the ground state, the $B'X_6$ and $B''X_6$ octahedra alternate in all directions.[11] In addition, the halide perovskites often crystallize in other three typical structures, tetragonal, orthorhombic, and hexagonal phases [Figs. 1(b)–1(d)].[39,40] Undoubtedly, it is deserving to identify the true crystal structure of Cs_2NaBiI_6, and it is significant to seek other similar iodide DPs to Cs_2NaBiI_6. In this paper, we evaluate the stability and explore the electronic structures and optical properties of a series of iodide $Cs_2B'BiI_6$ (B' = Li, Na and K) DP materials by first-principles calculations. These theoretical results provide a useful guide for the development of lead-free DP materials.

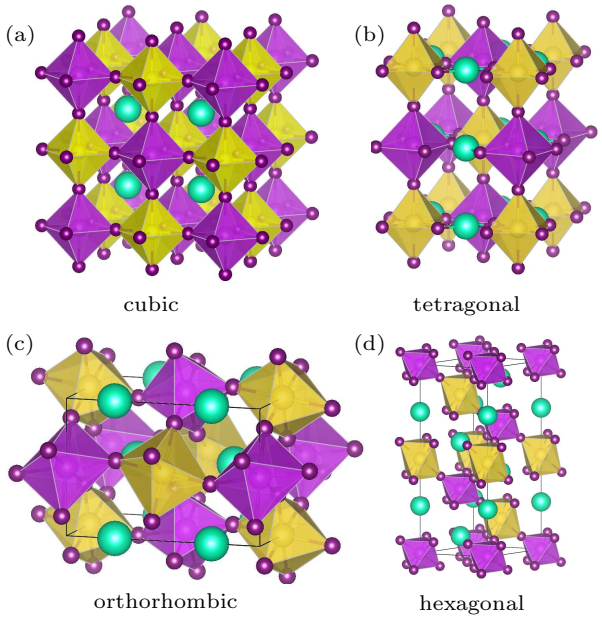


Fig. 1. The schematic crystal structure of hybrid halide $A_2^+B'^+B''^{3+}X_6$ DPs with different structural symmetry: (a) cubic, (b) tetragonal, (c) orthorhombic, and (d) hexagonal. The cyan, yellow, magenta, and purple balls denote the A, B', B'', and X atoms, respectively. The $B'X_6$ and $B''X_6$ octahedra are depicted in yellow and magenta colors.

2. Computational methods

All the theoretical calculations are based on the density functional theory as implemented in the Vienna *ab initio* simulation package (VASP) program[41] within the projector augmented wave method.[42] All calculations are performed by using the generalized-gradient approximation (GGA) electron exchange-correlation functional of Perdew–Burke–Ernzerhof (PBE) form.[43] The cutoff energy of 520 eV is used, and the k mesh is set to $0.15/2\pi$ Å^{-1} in reciprocal space. Electronic structures and optical property calculations have considered the spin-orbit coupling (SOC) effects. The structural models of $Cs_2B'BiI_6$ were initially built up by replacing atoms of the halide perovskite $MAPbI_3$ materials. As shown in Fig. 1, the cubic, tetragonal, orthorhombic, and hexagonal phases are considered in our simulations. The calculations are performed on primitive cells. All the lattice parameters and atomic positions of each DP compositions are fully relaxed until the force on each ion is less than 0.001 eV/Å and total energy convergence to 10^{-6} eV.

The optical absorption spectrum is calculated by the energy-related dielectric function:[44] $\varepsilon(\omega) = \varepsilon_1(\omega) + i\varepsilon_2(\omega)$, where $\varepsilon_1(\omega)$ and $\varepsilon_2(\omega)$ are the real and imaginary parts of the dielectric function, respectively. The optical absorption coefficient $\alpha(\omega)$ can be calculated by the following formula:[45]

$$\alpha(\omega) = \sqrt{2}\frac{\omega}{c}\left[\sqrt{\varepsilon_1^2(\omega)+\varepsilon_2^2(\omega)} - \varepsilon_1(\omega)\right]^{1/2}, \qquad (1)$$

where ω is the optical frequency, and c is the light speed in vacuum.

3. Results and discussion

3.1. Geometric stability

In order to evaluate the crystallographic stability of the perovskite materials ABX_3, two empirical parameters in the framework of the idealized solid sphere model are usually considered, that is the Goldschmidt tolerance factor t and the octahedral factor μ.[46] The Goldschmidt tolerance factor t is a commonly used and most successful empirical criteria, which is expressed as follows:[47]

$$t = \frac{R_A + R_X}{\sqrt{2}(R_B + R_X)}. \tag{2}$$

The octahedral factor μ is defined as $\mu = R_B/R_X$. R_A, R_B, and R_X are the effective ionic radii of the A cations, B cations, and X anions, respectively. Considering two types of B cations (B' and B'') in the $A_2B'^{+}B''^{3+}X_6$ DPs, the average value of the cation radius of B' and B'' is used as R_B. In general, the stable ranges of the DPs are $0.813 \leqslant t \leqslant 1.107$ and $0.414 \leqslant \mu \leqslant 0.732$.[48]

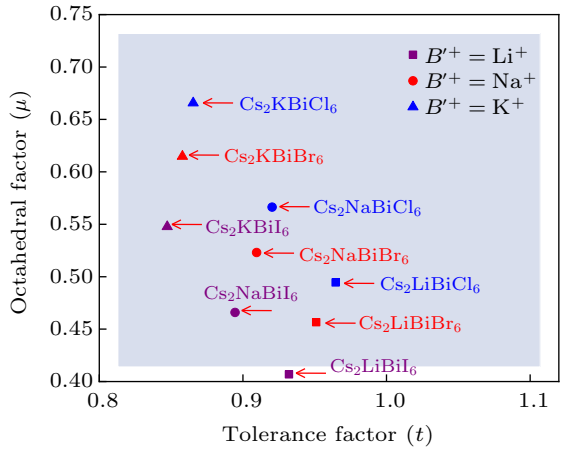


Fig. 2. Tolerance factor–octahedral structure map of the $Cs_2B'BiX_6$ (B' = Li, Na and K, X = Cl, Br, and I) DPs with effective tolerance factor (t) and octahedral factor (μ) as variables.

Using the Shannon ionic radii of the 12-coordinated Cs^+ ions and 6-coordinated B'^{+}, Bi^{3+}, and X^- ions,[49] we calculate the t and μ factors of the $Cs_2B'BiX_6$ (B' = Li, Na and K; X = Cl, Br and I) DPs. Figure 2 shows the distribution of the candidate $Cs_2B'BiX_6$ DPs in the map with t and μ variables. The shaded area indicates that the geometric structures of the DPs are stable. All the $Cs_2B'BiX_6$ DPs except Cs_2LiBiI_6 fall in the empirically stable region of DPs. The μ factor of Cs_2LiBiI_6 is 0.407, which is on the verge of the stable range of μ. Furthermore, the μ factors of the $LiBr_6$ and LiI_6 octahedra are 0.388 and 0.346, which are out of the stable criterion of μ. These results illustrate that $Cs_2LiBiBr_6$ and Cs_2LiBiI_6 are structurally less stable relative to other $Cs_2B'BiX_6$ DPs. In fact, among these predicted stable $Cs_2B'BiX_6$ DPs, only $Cs_2NaBiCl_6$, Cs_2KBiCl_6, and Cs_2NaBiI_6 have been experimentally synthesized to date.[19,20,22,23,31] As pointed out by Li *et al.*, both the t and μ factors are necessary but not sufficient conditions for the halide perovskite formability.[48] Therefore, it is necessary to assess the stability of $Cs_2B'BiI_6$ DPs based on other aspects.

3.2. Thermodynamic stability

We evaluate the ground state of the four possible structures of $Cs_2B'BiI_6$ by calculating the total energy (see Table 1). The calculated results manifest that the most favorable structure of $Cs_2B'BiI_6$ is the orthorhombic phase from an energetic viewpoint, which agrees with the experimental fact that the orthorhombic structure Cs_2NaBiI_6 has been synthesized.[31]

Table 1. The calculated total energy E (in units of eV/formula) of the four candidate structures of $Cs_2B'BiI_6$ DPs.

E	Cubic	Tetragonal	Orthorhombic	Hexagonal
Cs_2LiBiI_6	−27.2232	−26.0621	−27.2770	−27.2229
Cs_2NaBiI_6	−26.7910	−25.6030	−26.9356	−26.7903
Cs_2KBiI_6	−26.7950	−25.9185	−27.1217	−26.8720

In order to evaluate the thermodynamic stability of these $Cs_2B'BiI_6$ DPs, we calculate the formation energy and decomposition enthalpy. The binary phases are regarded as the synthesis reactants, and the Cs_3BiI_6 and $Cs_3Bi_2I_9$ ternary phases are possible decomposition products. Specifically, we consider one synthetic path of $2CsI + BiI_3 + B'I \rightarrow Cs_2B'BiI_6$ and two different decomposition paths of $Cs_2B'BiI_6 \rightarrow \frac{1}{2}Cs_3Bi_2I_9 + \frac{1}{2}CsI + B'I$ and $Cs_2B'BiI_6 \rightarrow \frac{2}{3}Cs_3BiI_6 + \frac{1}{3}BiI_3 + B'I$. The total energy of the reactants and decomposition products of the $Cs_2B'BiI_6$ DPs are presented in Table 2. The formation energy is defined as the energy differences between $Cs_2B'BiI_6$ DPs and the binary reactants: $\Delta E = E(Cs_2B'BiI_6) - (2E(CsI) + E(BiI_3) + E(B'I))$. The decomposition enthalpy (ΔH_d) is defined as the energy differences between the decomposition products and the $Cs_2B'BiI_6$ DPs according to the decomposition paths: $\Delta H_1 = \frac{1}{2}E(Cs_3Bi_2I_9) + \frac{1}{2}E(CsI) + E(B'I) - E(Cs_2B'BiI_6)$ and $\Delta H_2 = \frac{2}{3}E(Cs_3BiI_6) + \frac{1}{3}E(BiI_3) + E(B'I) - E(Cs_2B'BiI_6)$. A negative value of the formation energy represents an exothermic reaction process that will contribute to form a stable crystal structure, while a positive value of ΔH_d indicates the decomposition reaction is an endothermic process that will be unfavored for the decomposition of the $Cs_2B'BiI_6$ DPs, implying the thermodynamic stability. The $Cs_2B'BiI_6$ DPs is more stable with a lower value of the formation energy and a higher value of decomposition enthalpy.

Table 2. Calculated total energy E_{total} (eV/formula) of the reactants and decomposition products of the $Cs_2B'BiI_6$ DPs. The most stable crystal structures (the corresponding space groups are given in the parentheses) from the Materials Project crystal structure databases[50] are employed to calculate E_{total} of these materials.

Material	E_{total}	Material	E_{total}
BiI_3 ($R\bar{3}$)	−10.3862	CsI ($Fm\bar{3}m$)	−5.5095
LiI ($Fm\bar{3}m$)	−5.8215	Cs_3BiI_6 ($Fm\bar{3}m$)	−26.4966
NaI ($Fm\bar{3}m$)	−5.4033	$Cs_3Bi_2I_9$ ($P6_3/mmc$)	−37.7680
KI ($Fm\bar{3}m$)	−5.5652		

The formation energy of the cubic, tetragonal, orthorhombic, and hexagonal phases $Cs_2B'BiI_6$ DPs are shown in Fig. 3. The orthorhombic phase $Cs_2B'BiI_6$ displays negative formation energies, while all the other phases $Cs_2B'BiI_6$ DPs show positive formation energies. Therefore, only the orthorhombic phase meets the thermodynamic stable conditions, and the other three crystal structures are unstable. The theoretically calculated result is in line with previous reports on the cubic phase Cs_2NaBiI_6.[38] Considering the Cs_2NaBiI_6 has been experimentally synthesized in the orthorhombic structure,[31] we suspect that orthorhombic Cs_2LiBiI_6 and Cs_2KBiI_6 can also be synthesized by the corresponding binary compounds within an exothermic reaction process.

The calculated results of the decomposition enthalpy of $Cs_2B'BiI_6$ along two representative decomposition paths are shown in Fig. 4. The products of the first decomposition path are $Cs_3Bi_2I_9$, CsI and $B'I$, while those of the second case are Cs_3BiI_6, BiI_3 and $B'I$. The ΔH_1 are all negative values for all the four considered phases, which indicate that even if the $Cs_2B'BiI_6$ DPs have been synthesized, they will spontaneously decompose to $Cs_3Bi_2I_9$ and other binary compositions. By contrast, all the DPs except the tetragonal phase show positive ΔH_2 values, illustrating that other three phases of $Cs_2B'BiI_6$ DPs will much more stable than the tetragonal phase. All the orthorhombic phases show lower values of ΔH_1 and higher values of ΔH_2, which is consistent with the results of the formation energy, so that the orthorhombic phase will more stable than other three crystal structures. In addition, the orthorhombic phase of Cs_2LiBiI_6 exhibits the largest negative value of ΔH_1 and the smallest positive value of ΔH_2 with respect to the same orthorhombic phase Cs_2NaBiI_6 and Cs_2KBiI_6, indicates that orthorhombic Cs_2LiBiI_6 is less stable relative to other two counterpart DPs. The thermodynamic stability is well consistent with the geometric stability, so that the stable orthorhombic $Cs_2B'BiI_6$ DPs may be synthesized in experiments.[31] Hereafter, we will only discuss the orthorhombic phase $Cs_2B'BiI_6$.

Owing to the orthorhombic structures of $Cs_2B'BiI_6$ are constructed from the $MAPbI_3$ by replacing MA group with Cs ions and Pb ions with B' and Bi ions,[31,34] the spatial symmetry of B-site Pb ions have split to two different B' and Bi ions, which form the rock-salt order in the perovskite B sites. Then the orthorhombic space group $Pnma$ of $MAPbI_3$ formally changes to the monoclinic space group $P2_1/n$.[51] The Wyckoff positions of Bi and B' (B' = Li, Na, K) are $2c$ (0.5, 0.5, 0) and $2d$ (0, 0, 0), which have unchanged in the monoclinic representation. The Cs and I atoms occupy the Wyckoff positions of $4e$. The crystallographic data of the orthorhombic $Cs_2B'BiI_6$ DPs are shown in Table 3. The B'–I (B' = Na or K) bond lengths are longer than those of the Bi–I bond length. Other lead-free DPs also have similar bond lengths, for instance, $Cs_2AgSbCl_6$ (Ag–Cl = 2.72 Å; Sb–Cl = 2.63 Å).[52]

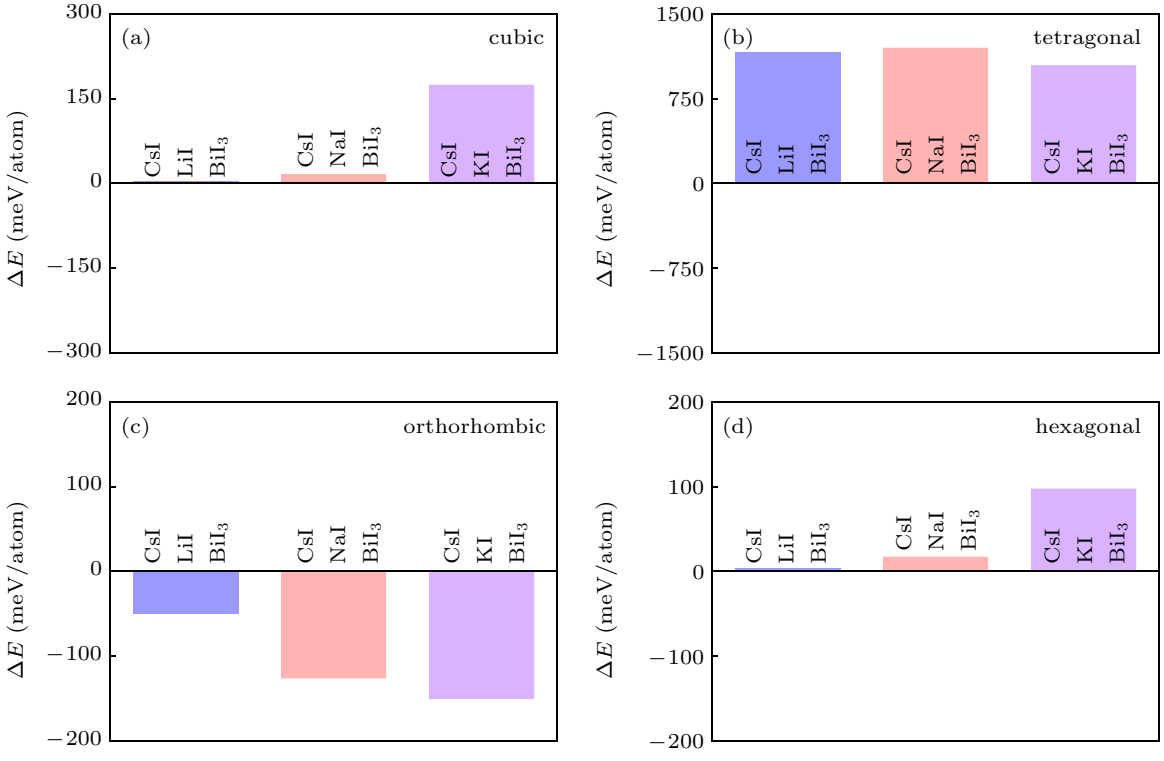


Fig. 3. Calculated formation energy of the $Cs_2B'BiI_6$ DPs with different crystal structures: (a) cubic, (b) tetragonal, (c) orthorhombic, (d) hexagonal. The blue, orange and purple bars represent the result of Cs_2LiBiI_6, Cs_2NaBiI_6 and Cs_2KBiI_6, respectively.

Table 3. Calculated lattice parameters, atomic positions, cell volumes and bond distances (B'–I and Bi–I) of $Cs_2B'BiI_6$ DPs.

	Cs_2LiBiI_6	Cs_2NaBiI_6	Cs_2KBiI_6
a (Å)	8.395	8.622	8.793
b (Å)	8.432	8.929	9.373
c (Å)	12.804	12.509	12.758
Volume (Å^3)	906.287	963.171	1051.519
Cs	(−0.493, 0.025, 0.249)	(−0.479, 0.066, 0.249)	(−0.471, 0.079, 0.248)
I1	(0.296, 0.191, 0.991)	(0.305, 0.208, 0.970)	(0.324, 0.218, 0.952)
I2	(−0.192, 0.296, 0.0120)	(−0.205, 0.304, 0.035)	(−0.209, 0.320, 0.046)
I3	(−0.435, 0.500, 0.755)	(−0.435, 0.500, 0.755)	(−0.405, 0.522, 0.766)
B'–I (Å)	3.297 × 2	3.272 × 2	3.570 × 2
	2.974 × 2	3.247 × 2	3.562 × 2
	2.967 × 2	3.244 × 2	3.502 × 2
Bi–I (Å)	3.114 × 2	3.118 × 2	3.120 × 2
	3.113 × 2	3.114 × 2	3.119 × 2
	3.110 × 2	3.110 × 2	3.107 × 2

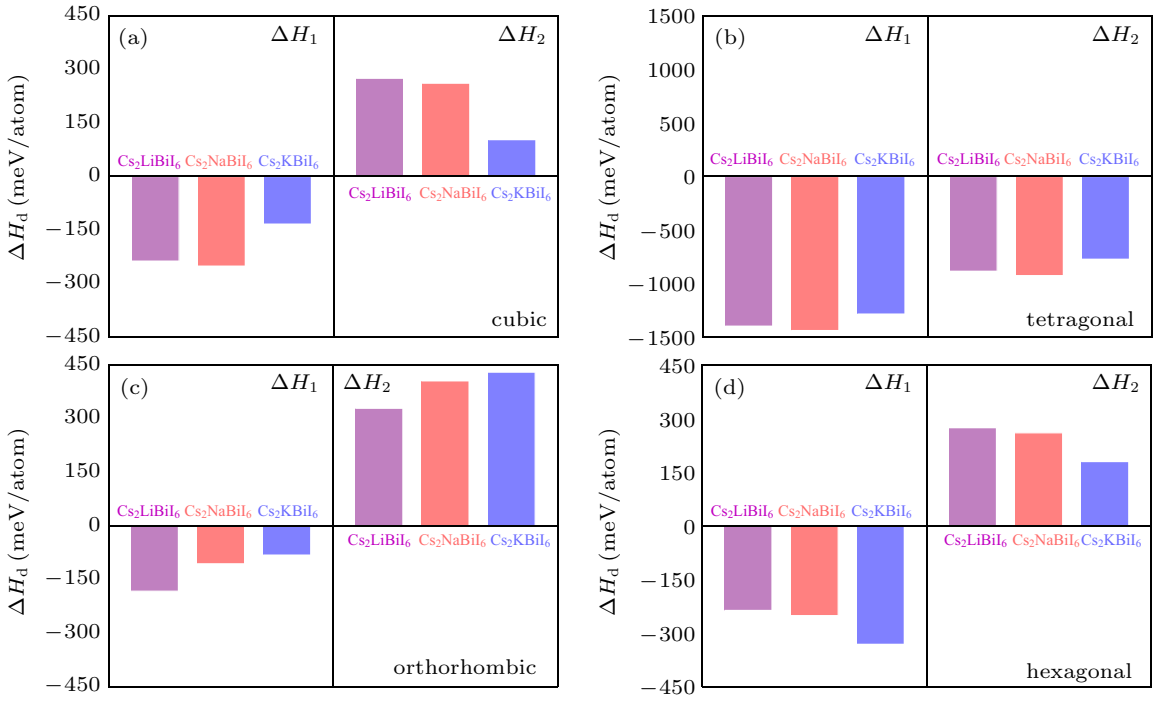


Fig. 4. Calculated decomposition enthalpy ΔH_d of $Cs_2B'BiI_6$ double perovskites along two representative decomposition pathways: (a) cubic, (b) tetragonal, (c) orthorhombic, and (d) hexagonal.

3.3. Mechanical stability

Elastic constants are important parameters to measure the bearing capacity of materials, and could conduce to evaluate the mechanical stability. In this study, the elastic constants C_{ij} are estimated in accordance with the relationship between strain and volume,[53] which are listed in Table 4. According to the mechanical stability criterion of monoclinic crystals,[54] Cs_2LiBiI_6 material does not meet the mechanical stability, while Cs_2NaBiI_6 and Cs_2KBiI_6 fulfil the mechanical stability conditions. Therefore, the geometric, thermodynamic, and mechanical stabilities reveal that the orthorhombic Cs_2LiBiI_6 material is less stable relative to the isostructural Cs_2NaBiI_6 and Cs_2KBiI_6 DPs.

Employing the Voigt–Reuss–Hill approximations, the mechanical properties, such as the bulk modulus (B) and the shear modulus (G) can be calculated from the elastic matrix C_{ij},[55,56] while the Young's modulus (E) and Poisson's ratio (ν) are calculated by the following formula: $E = 9BG/(3B+G)$, and $\nu = (3B-G)/[2(3B+G)]$.[54] The small bulk moduli B manifest that the $Cs_2B'BiI_6$ are easily compressible materials, which are also easier to be deformed by tensile stress for the reason of the weak bond strength. Furthermore, the shear moduli G of $Cs_2B'BiI_6$ are smaller with respect to Cs_2AgBiI_6,[57] and indicates its stronger capacity to shape change through distortion under shear loading. The calculated Poisson's ratios are bigger than 0.3, and the Pugh's ratios B/G are larger than the critical value of 1.75, which means these $Cs_2B'BiI_6$ DP materials possess good ductility. The mechanical properties demonstrate that the $Cs_2B'BiI_6$ DPs may be used as flexible materials.[57]

Table 4. Calculated elastic constants C_{ij} (GPa), bulk modulus B (GPa), shear modulus G (GPa), Young's modulus E (GPa), Poisson's ratio ν, Pugh's ratio (B/G) of $Cs_2B'BiI_6$. The subscripts V and R of the moduli denote results from the Voigt and Reuss models, while B and G moduli without subscripts from the Voigt–Reuss–Hill approximations defined as the average of the Reuss and Voight values, respectively.

	Cs_2LiBiI_6	Cs_2NaBiI_6	Cs_2KBiI_6		Cs_2LiBiI_6	Cs_2NaBiI_6	Cs_2KBiI_6
C_{11}	18.90	12.46	9.72	C_{35}	2.38	0.46	1.43
C_{22}	8.57	14.04	14.04	C_{46}	0.58	0.42	−0.40
C_{33}	7.72	17.41	16.58	B_V	12.046	10.659	8.876
C_{44}	5.18	5.08	3.69	B_R	12.014	10.391	8.492
C_{55}	4.41	4.55	2.50	B	12.030	10.525	8.684
C_{66}	4.58	4.57	4.22	G_V	2.739	4.033	3.453
C_{12}	9.61	8.43	7.59	G_R	7.529	3.667	2.932
C_{13}	9.09	9.26	6.22	G	5.134	3.850	3.193
C_{23}	17.91	8.32	5.96	E	13.484	10.295	8.533
C_{15}	0.46	0.35	−0.05	ν	0.313	0.337	0.336
C_{25}	−2.69	0.40	−0.56	B/G	2.343	2.734	2.720

3.4. Electronic structure and optical properties

In order to better understand the electronic structure of the $Cs_2B'BiI_6$, the band structure and the partial density of states (DOS) have been calculated. The band gaps of Cs_2LiBiI_6, Cs_2NaBiI_6 and Cs_2KBiI_6 calculated within GGA are 2.26 eV, 2.37 eV, and 2.79 eV, respectively. By considering the SOC effect, the band gaps are significantly reduced to 1.51 eV, 1.73 eV and 1.99 eV, respectively The theoretically calculated band gap value (1.73 eV) of Cs_2NaBiI_6 agrees well with the experimentally derived value (1.66 eV).[31] Without considering the SOC effect, $Cs_2B'BiI_6$ DPs are predicted to be indirect band gap semiconductors. As shown in Fig. 5, Cs_2LiBiI_6 is predicted to be a direct band gap semiconductor when the SOC effect has been considered, where the valence band maximum (VBM) and the conduction band minimum (CBM) are located at the same Γ point. By contrast, Cs_2NaBiI_6 and Cs_2KBiI_6 still are indirect band gap semiconductors. The band gap values of $Cs_2B'BiI_6$ increase in the order of increasing ions radium from Li, Na to K, which are similar to the cases of chloride $Cs_2B'BiCl_6$ DPs.[11] At the same time, the increasing size of B' ion from Li, Na to K will lead to the $B'I_6$ octahedron expand and the BiX_6 octahedron contract, which result in an increase of the interaction between Bi 6p and I 5p orbitals and lead to a raise of VBM. As shown in the partial DOS, the VBM predominantly arise from the I 5p orbital, while the CBM is contributed by strong hybridizations of Bi 6p and I 5p states. Furthermore, the strong SOC interactions induced energy level splitting of the Bi 6p states will give rise to the decrease of the CBM position and the reduction of the band gap. Replacing Cl by I significantly lower the CBM and raise the VBM due to the interaction between Bi^{3+} and I ions,[11] resulting in the band gap shrinkage from 3.41 eV ($Cs_2NaBiCl_6$)[29] to 1.66 eV (Cs_2NaBiI_6).[31]

The mobility of the carriers is one key parameter for optoelectronic applications. The effective mass of electrons (m_e^*) and holes (m_h^*) at the CBM and VBM can be derived from

$$m^* = \hbar^2 \left[\partial^2 \varepsilon(k) / \partial k^2 \right]^{-1}, \quad (3)$$

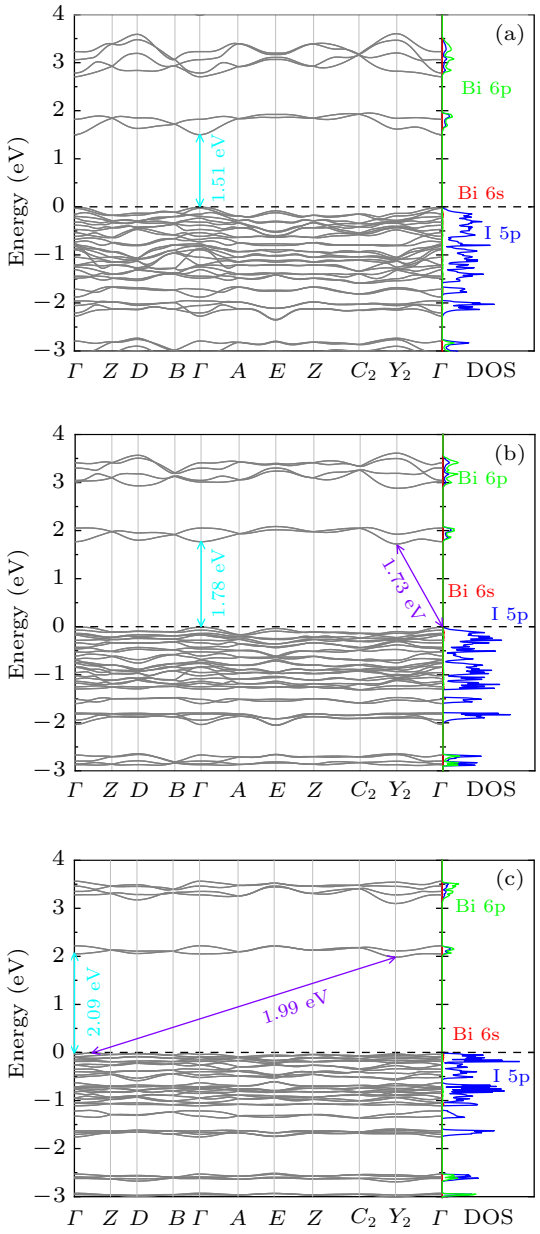


Fig. 5. Band structures and the partial DOS of orthorhombic $Cs_2B'BiI_6$ DPs calculated within GGA + SOC: (a) Cs_2LiBiI_6, (b) Cs_2NaBiI_6, (c) Cs_2KBiI_6. The arrows depict the direct and indirect band gaps. The partial DOS of the Bi 6s, 6p, and I 5p states are drawn with red, green, and blue lines, respectively.

Table 5. The effective masses of electrons (m_e^*) in CBM and holes (m_h^*) in VBM, reduced effective masse of the carriers (m_r^*), static dielectric constant (ε_{optic}) and exciton binding energy (E_b) of $Cs_2B'BiI_6$.

Material	Valence band			Conduction band			$\langle m_h^* \rangle$	$\langle m_e^* \rangle$	$\langle m_r^* \rangle$	ε_{optic}	E_b
	m_{xx}^*	m_{yy}^*	m_{zz}^*	m_{xx}^*	m_{yy}^*	m_{zz}^*					
Cs_2LiBiI_6	2.343	2.842	1.269	0.655	0.629	0.600	1.9149	0.6272	0.4725	5.2536	0.2321
Cs_2NaBiI_6	2.573	5.861	2.108	1.185	0.625	0.660	2.9023	0.7578	0.6009	5.1902	0.3025
Cs_2KBiI_6	2.735	2.286	9.374	2.063	0.989	1.144	3.2976	1.2658	0.9147	4.6344	0.5775

where $\hbar$ is reduced Planck constant, and $\varepsilon(k)$ is the orbit eigenvalue. The average effective mass values of the carriers are defined as: $m_I^* = 3/(1/m_{xx} + 1/m_{yy} + 1/m_{zz})$, I = e or h.[37] Furthermore, the exciton binding energy (E_b) can be obtained from the following formula:[58,59]

$$E_b \approx 13.56 \frac{m_r^*}{m_e} \frac{1}{\varepsilon_{optic}^2}, \tag{4}$$

where m_r^* is the reduced effective mass of electrons and holes, and ε_{optic} is the static dielectric constant.

As shown in Table 5, the effective masses of electrons (holes) of Cs_2LiBiI_6, Cs_2NaBiI_6, and Cs_2KBiI_6 are 0.6272 m_e (1.9149 m_e), 0.7578 m_e (2.9023 m_e), and 1.2658 m_e (3.2976 m_e), respectively, where m_e stands for the electron static mass. The effective masses of electrons and holes increase along with the increasing atomic radius, implying lower carrier mobility, because the effective mass and conductivity show an inverse proportional relationship.[60] The exciton binding energies of Cs_2LiBiI_6 (Cs_2NaBiI_6, Cs_2KBiI_6) are 0.2321 eV (0.3025 eV, 0.5775 eV), which are comparable to those of the low-dimensional organic tin bromide perovskites[37] and 3D/2D hybrid lead-halide perovskites $(C_4H_9NH_3)_2PbX_4$.[58] These results imply that $Cs_2B'BiI_6$ DPs materials with weaker exciton binding energy are suitable for solar cell applications.

To further investigate the light harvesting capacity of these $Cs_2B'BiI_6$ DPs, we calculate the optical absorption coefficients. As shown in Fig. 6, the light absorption of Cs_2LiBiI_6 (Cs_2NaBiI_6, Cs_2KBiI_6) increases rapidly above 1.51 eV (1.73 eV, 1.99 eV), which are consist with the band gap determined by electronic transitions from the top of valence bands to the bottom of conduction bands. Especially, the light absorption efficiency is significantly improved in the visible light region, which reaches an order of 10^6 cm^{-1}, overperforms the organic–inorganic hybrid perovskite materials $MAPbI_3$.[61,62] The characteristic peaks of absorption coefficients are mainly derived from the transitions from I 5p to Bi 6p states, similar to that of the lead halide perovskites. According to the band dispersions illustrated in Fig. 5, although the band gaps of the Cs_2NaBiI_6 and Cs_2KBiI_6 are indirect type, the energies of the conduction bands are very close at Γ and Y_2 points, implying strong direct transitions, which are beneficial for the optical performances. In addition, the absorption coefficients along three incident directions are very close, implying the $Cs_2B'BiI_6$ DPs are almost isotropic. The excellent optical absorption performances demonstrate $Cs_2B'BiI_6$ DPs can be effective solar energy absorbers in the visible light spectrum.

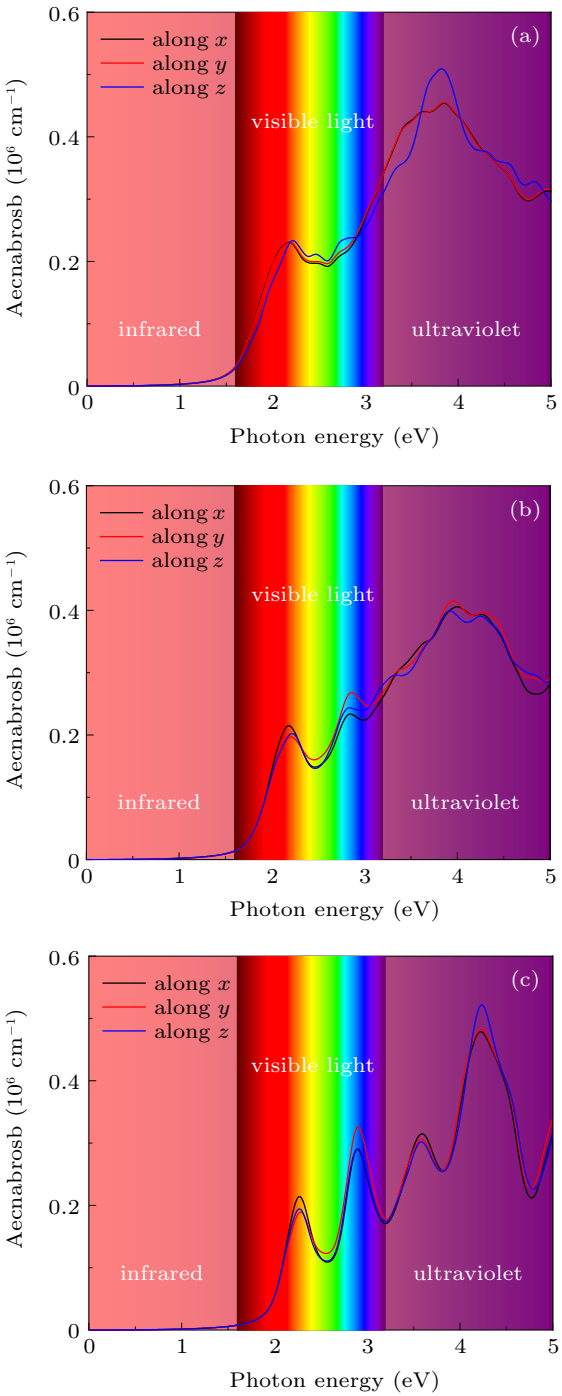


Fig. 6. Optical absorption spectrum of orthorhombic $Cs_2B'BiI_6$: (a) Cs_2LiBiI_6, (b) Cs_2NaBiI_6, (c) Cs_2KBiI_6.

4. Conclusions

In summary, the geometric stability, thermodynamic stability, mechanical stability, electronic structure, and optical properties of the $Cs_2B'BiI_6$ (B' = Li, Na and K) DPs were studied by the first-principles calculations. By comprehensive evaluations of the tolerance factor t, octahedral factor μ, formation energy, decomposition enthalpy, and mechanical stability, the stable orthorhombic phase of $Cs_2B'BiI_6$ has been identified out of four different crystal structures (cubic, tetragonal, orthorhombic, and hexagonal phases). Furthermore, the orthorhombic Cs_2LiBiI_6 is less stable than the isostructural Cs_2NaBiI_6 and Cs_2KBiI_6, which is consistent with the experimental fact that the orthorhombic structure Cs_2NaBiI_6 has been synthesized. The orthorhombic Cs_2LiBiI_6 show direct band gap characteristics, while Cs_2NaBiI_6 and Cs_2KBiI_6 have indirect band gaps, and all of them show weaker exciton binding energies and good light absorption performances in the visible light region. According to the good stability, suitable band gap, and excellent optoelectronic properties, the orthorhombic Cs_2NaBiI_6 and Cs_2KBiI_6 can be used as promising lead-free solar-cells materials for optoelectronic applications.

References

[1] Quan L N, Rand B P, Friend R H, Mhaisalkar S G, Lee T W and Sargent E H 2019 *Chem. Rev.* **119** 7444
[2] Bai S, Da P, Li C, Wang Z, Yuan Z, Fu F, Kawecki M, Liu X, Sakai N, Wang J T W, Huettner S, Buecheler S, Fahlman M, Gao F and Snaith H J 2019 *Nature* **571** 245
[3] Best Research-Cell Efficiency Chart https://www.nrel.gov/pv/assets/pdfs/best-research-cell-efficiencies.20200104.pdf
[4] Ke W and Kanatzidis M G 2019 *Nat. Commun.* **10** 965
[5] Jena A K, Kulkarni A and Miyasaka T 2019 *Chem. Rev.* **119** 3036
[6] Shamsi J, Urban A S, Imran M, De Trizio L and Manna L 2019 *Chem. Rev.* **119** 3296
[7] Jiang X and Yin W J 2020 *Chin. Phys. B* **29** 028803
[8] Yang J, Zhang P, Wang J and Wei S H 2020 *Chin. Phys. B* **29** 108401
[9] Jellicoe T C, Richter J M, Glass H F J, Tabachnyk M, Brady R, Dutton S E, Rao A, Friend R H, Credgington D, Greenham N C and Böhm M L 2016 *J. Am. Chem. Soc.* **138** 2941
[10] Swarnkar A, Ravi V K and Nag A 2017 *ACS Energy Lett.* **2** 1089
[11] Zhao X G, Yang J H, Fu Y, Yang D, Xu Q, Yu L, Wei S H and Zhang L 2017 *J. Am. Chem. Soc.* **139** 2630
[12] Xiao Z, Du K Z, Meng W, Wang J, Mitzi D B and Yan Y 2017 *J. Am. Chem. Soc.* **139** 6054
[13] Zhao X G, Yang D, Ren J C, Sun Y, Xiao Z and Zhang L 2018 *Joule* **2** 1662
[14] Li T, Zhao X, Yang D, Du M H and Zhang L 2018 *Phys. Rev. Appl.* **10** 041001
[15] Zhao X G, Yang D, Sun Y, Li T, Zhang L, Yu L and Zunger A 2017 *J. Am. Chem. Soc.* **139** 6718
[16] Xu Q, Yang D, Lv J, Sun Y Y and Zhang L 2018 *Small Methods* **2** 1700316
[17] Chu L, Ahmad W, Liu W, Yang J, Zhang R, Sun Y, Yang J and Li X 2019 *Nano-Micro Lett.* **11** 16
[18] Xiao Z, Meng W, Wang J, Mitzi D B and Yan Y 2017 *Mater. Horizons* **4** 206
[19] Morss L R, Siegal M, Stenger L and Edelstein N 1970 *Inorg. Chem.* **9** 1771
[20] Barbier P, Drache M, Mairesse G and Ravez J 1982 *J. Solid State Chem.* **42** 130
[21] Flerov I N, Gorev M V, Aleksandrov K S, Tressaud A, Grannec J and Couzi M 1998 *Mater. Sci. Eng. R Reports* **24** 81
[22] Smit W M A, Dirksen G J and Stufkens D J 1990 *J. Phys. Chem. Solids* **51** 189
[23] Pelle F, Blanzat B and Chevalier B 1984 *Solid State Commun.* **49** 1089
[24] McClure E T, Ball M R, Windl W and Woodward P M 2016 *Chem. Mater.* **28** 1348
[25] Slavney A H, Hu T, Lindenberg A M and Karunadasa H I 2016 *J. Am. Chem. Soc.* **138** 2138
[26] Filip M R, Hillman S, Haghighirad A A, Snaith H J and Giustino F 2016 *J. Phys. Chem. Lett.* **7** 2579
[27] Shi H and Du M H 2015 *Phys. Rev. Appl.* **3** 054005
[28] Majher J D, Gray M B, Strom T A and Woodward P M 2019 *Chem. Mater.* **31** 1738
[29] Zhou J, Rong X, Zhang P, Molokeev M S, Wei P, Liu Q, Zhang X and Xia Z 2019 *Adv. Opt. Mater.* **7** 1801435
[30] Yao M M, Wang L, Yao J S, Wang K H, Chen C, Zhu B S, Yang J N, Wang J J, Xu W P, Zhang Q and Yao H B 2020 *Adv. Opt. Mater.* **8** 1901919
[31] Zhang C, Gao L, Teo S, Guo Z, Xu Z, Zhao S and Ma T 2018 *Sustain. Energy Fuels* **2** 2419
[32] Peedikakkandy L, Chatterjee S and Pal A J 2020 *J. Phys. Chem. C* **124** 10878
[33] Li P, Gao W, Ran C, Dong H, Hou X and Wu Z 2019 *Phys. Status Solidi* **216** 1900567
[34] Cheng P, Wu T, Li Y, Jiang L, Deng W and Han K 2017 *New J. Chem.* **41** 9598
[35] Yang F, Wang C, Pan Y, Zhou X, Kong X and Ji W 2019 *Chin. Phys. B* **28** 056402
[36] Diao X F, Tang Y L and Xie Q 2019 *Chin. Phys. B* **28** 017802
[37] Lei J H, Tang Q, He J and Cai M Q 2021 *Chin. Phys. B* **30** 038102
[38] Zhao S, Yamamoto K, Iikubo S, Hayase S and Ma T 2018 *J. Phys. Chem. Solids* **117** 117
[39] Baikie T, Fang Y, Kadro J M, Schreyer M, Wei F, Mhaisalkar S G, Graetzel M and White T J 2013 *J. Mater. Chem. A* **1** 5628
[40] Thind A S, Huang X, Sun J and Mishra R 2017 *Chem. Mater.* **29** 6003
[41] Kresse G and Furthmüller J 1996 *Phys. Rev. B* **54** 11169
[42] Blöchl P E 1994 *Phys. Rev. B* **50** 17953
[43] Perdew J P, Burke K and Ernzerhof M 1996 *Phys. Rev. Lett.* **77** 3865
[44] Gajdoš M, Hummer K, Kresse G, Furthmüller J and Bechstedt F 2006 *Phys. Rev. B* **73** 045112
[45] Huang X, Paudel T R, Dong S and Tsymbal E Y 2015 *Phys. Rev. B* **92** 125201
[46] Travis W, Glover E N K, Bronstein H, Scanlon D O and Palgrave R G 2016 *Chem. Sci.* **7** 4548
[47] Goldschmidt V M 1926 *Naturwissenschaften* **14** 477
[48] Li C, Lu X, Ding W, Feng L, Gao Y and Guo Z 2008 *Acta Crystallogr. Sect. B Struct. Sci.* **64** 702
[49] Shannon R D 1976 *Acta Crystallogr. Sect. A* **32** 751
[50] Jain A, Ong S P, Hautier G, Chen W, Richards W D, Dacek S, Cholia S, Gunter D, Skinner D, Ceder G and Persson K A 2013 *APL Mater.* **1** 011002
[51] Gómez-Pérez A, Pérez-Flores J C, Ritter C, Boulahya K, Castro G R, García-Alvarado F and Amador U 2014 *J. Appl. Crystallogr.* **47** 745
[52] Volonakis G, Filip M R, Haghighirad A A, Sakai N, Wenger B, Snaith H J and Giustino F 2016 *J. Phys. Chem. Lett.* **7** 1254
[53] Dar S A, Srivastava V and Sakalle U K 2017 *Mater. Res. Express* **4** 086304
[54] Wu Z J, Zhao E J, Xiang H P, Hao X F, Liu X J and Meng J 2007 *Phys. Rev. B* **76** 054115
[55] Hill R 1952 *Proc. Phys. Soc. Sect. A* **65** 349
[56] Pu C Y, Yu R M, Wang T, Xüe Z Y, Zhu Y S and Zhou D W 2021 *Chin. Phys. B* **30** 017102
[57] Su J, Zhang Z, Hou J, Liu M, Lin Z, Hu Z, Chang J and Hao Y 2019 *Adv. Theory Simulations* **2** 1900164
[58] Wang D, Wen B, Zhu Y N, Tong C J, Tang Z K and Liu L M 2017 *J. Phys. Chem. Lett.* **8** 876
[59] Jong U G, Yu C J, Ri J S, Kim N H and Ri G C 2016 *Phys. Rev. B* **94** 1
[60] Khan I, Shahab, Haq I U, Ali A, Ali Z and Ahmad I 2021 *J. Electron. Mater.* **50** 456
[61] Xing G, Mathews N, Sun S, Lim S S, Lam Y M, Graẗzel M, Mhaisalkar S and Sum T C 2013 *Science.* **342** 344
[62] Kim H S, Lee C R, Im J H, Lee K B, Moehl T, Marchioro A, Moon S J, Humphry-Baker R, Yum J H, Moser J E, Grätzel M and Park N G 2012 *Sci. Rep.* **2** 591